Available online at http://scik.org
Commun. Math. Biol. Neurosci. 2026, 2026:57
https://doi.org/10.28919/cmbn/9761
ISSN: 2052-2541

BAYESIAN SPATIO-TEMPORAL MODEL SIMULATION OF CLIMATIC INFLUENCES ON MALARIA-TYPHOID DYNAMICS

EDMOND MUDAHOGORA KAZUNGU[1,*], ATINUKE OLUSOLA ADEBANJI[2], DENIS NDANGUZA[3], GIDEON MUTIE KIKUVI[4]

[1]Pan African University Institute for Basic Sciences Technology and Innovation, Nairobi, Kenya

[2]Kwame Nkrumah University of Science and Technology, Kumasi, Ghana

[3]University of Rwanda, College of Science and Technology, Kigali, Rwanda

[4]Jomo Kenyatta University of Agriculture and Technology, Nairobi, Kenya

Abstract. Typhoid and Malaria are among the world's biggest health challenges, with the Sub-Saharan Africa being the most affected. Although typhoid and malaria have different causes and modes of spread, they both have similar symptoms. Despite historical attempts to model the co-occurrence of malaria and typhoid have achieved some success, they often overlooked the inter-connectedness between climatic factors, spatio-temporal disease transmission dynamics, and co-infection. The aim of this study was to develop a Bayesian hierarchical spatio-temporal model for the joint analysis of malaria and typhoid, which includes both specific and shared spatio-temporal effects under an influence of climatic factors. Parameters for variables such as temperature, precipitation and humidity were estimated under a simulation study using Bayesian inference through the R-INLA approach which serves as an alternative to MCMC since it tackles even intractable integrals. After developing the model, we assessed the properties of the estimators. Plots alongside statistics such as RMSE, variance, Shapiro, mean Z, Skewness, Kurtosis among others were done. The estimator was unbiased, asymptotically normal, asymptotically efficiency and consistent. For increasing observations beyond 1,000 the bias, standard deviation and root mean squared errors (RMSE) decrease hence the sample size was sufficient. Thanks to the simulations, it was observed

*Corresponding author

E-mail address: mudahogora.edmond@students.jkuat.ac.ke

Received January 01, 2026

that temperature had a high impact on the co-infection than other variables while lower precipitation was associated with increased risk. The structured spatial effect revealed a bigger influence on the disease co-infection than other spatial and temporal components.

Keywords: co-infection; Bayesian hierarchies; climatic factors; integrated nested Laplace approximation; spatio-temporal dynamics.

2020 AMS Subject Classification: 62F15, 62J12, 86A08, 62M10.

1. INTRODUCTION

Malaria is a parasitic disease spread by the bites of Anopheles mosquitoes carrying the Plasmodium species [1]. *Plasmodium vivax, Plasmodium falciparum, Plasmodium malariae, Plasmodium Ovale* and *Plasmodium knowlesi* are the five species into which this plasmodium is classified [2]. It poses a serious threat to public health because it is the cause of many deaths in the endemic tropical regions of the world. In 2018, around half of the world's population was at danger of malaria. Sub-Saharan Africa is home to the majority of cases and fatalities that have been reported [3].

Conversely, *Salmonella Enterica Serotypes Typhi* (S. typhi) and *Paratyphi* (*S. paratyphi* A, B, and C) are the causative agents of typhoid fever. The most prevalent salmonella serotype that causes typhoid fever is *S.typhi* [4]. Consuming contaminated food, beverages or contact with waste is a common method of acquiring typhoid [5]. Malaria and typhoid fever have similar associations despite having distinct causes and modes of transmission. Since typhoid and malaria have comparable signs and symptoms such as fever, headache, vomiting, diarrhoea, stomachache, abdominal and muscle pain clinical diagnosis is a challenge which may lead to the mismanagement of the two illnesses [4].

The shared social variables are critical to the spread of both typhoid fever and malaria. Thus, living in a region where typhoid fever and malaria are both endemic puts residents at risk of contracting the diseases simultaneously. Particularly in tropical regions where malaria is widespread, the co-infection between the malaria parasite and Salmonella typhi is frequent. Some people think that malaria can develop to typhoid fever due to the frequent discovery of high antibody titre of these Salmonella serotypes in malaria patients. Therefore, even in the absence

of sufficient laboratory diagnosis for malaria, some individuals treat both typhoid fever and malaria simultaneously once they have strong antibody titre for Salmonella serotypes [6].

The first account of the connection between typhoid and malaria was discovered by a US army physician Joseph J. Woodward (1833–1884) in 1862, on this date during the American Civil War. Young troops with severe illnesses that appeared to be typhoid fever rather than a novel disease were found to have both malaria and typhoid fever. Later, towards the end of 19th century, laboratory testing disproved the earlier notion by showing that it was either one disease or another, or very infrequently, a coinfection with both Salmonella typhi and the Plasmodium species [6].

There is a growing recognition that climate change is a complex factor contributing to a range of detrimental effects on health [7]. Climate can affect health in a number of ways, including temperature changes, extreme weather events, air pollution, and the escalation of vector-food, and water-borne disease as well as food shortages. Health may also be impacted by climate change as a result of socioeconomic disruption and human migration [8].

Variations in temperature, precipitation, rainfall, sunlight, humidity and other climatic factors might affect the ability of disease pathogens and hosts to survive, reproduce, or spread, as well as the accessibility and mode of transmission of these agents in the environment. Such consequences often manifest as changes in the seasonal and geographic patterns of human infectious illnesses, as well as in the frequency and intensity of their outbreaks. The spatiotemporal distribution of disease vectors is influenced by temperature. As the temperature rises, insects from low latitude regions may find new homes in high altitude and mid latitude regions, which might result in the spread of diseases or an extension of the geographic area [9].

However, as the temperature rises over 33–39 ^{0}C, the growth of the malaria parasites (Plasmodium falciparum and Plasmodium vivax) stops. The extrinsic incubation period (EIP) and reproduction of infections are also impacted by temperature rise. For instance, the EIP of P. falciparum's is shortened from 26 days at 20 ^{0}C to 13 days at 25 ^{0}C. In Anopheline mosquitoes, humidity has also been shown to influence the growth of malarial parasites [9]. Briefly, typhoid and malaria, like the majority of other vector-borne illnesses, are characterized by spatiotemporal fluctuations or changes brought on by demographic, socioeconomic, climatic, and

geographic variables. These variables may be utilized to pinpoint hotspots and determine the spatiotemporal patterns of illness in order to support efficient resource allocation, efficient disease assessment, and efficient disease control [10].

Infectious diseases spread by water or food are linked to meteorological parameters including temperature and precipitation. Salmonella infections, cholera, bacillary dysentery, and other diarrheal illnesses are examples of enteric infections linked to temperature and precipitation. Typhoid and paratyphoid fever epidemics often happen in the wet and dry, and their seasonal pattern changes depending on latitude, suggesting that meteorological variables might be involved in their spread [11].

Increased temperature and precipitation have been linked to increased Salmonella growth and reproduction, water source pollution and diffusion, host lifestyle and immunity, and an increased risk of water and food-borne diarrhea associated diseases like typhoid and paratyphoid fever. Countless research investigations have documented regional variations in the interactions between climate and Salmonella, suggesting the presence of distinct infection patterns [11].

The environmental sciences and epidemiology are well known for their use in spatio-temporal analysis. Generally, the information gathered from locations in space during a specific period of time is not independent. These data are time and space dependent, meaning that observations from one site at a given time often show values that are comparable to those from surrounding locations at the same time. Failing to account for the violation of temporal and geographical independence between observations would lead to biased and inconsistent estimates. This sums up the advances in spatio-temporal analysis, which introduce randomness into the concept of spatial and temporal effects [12].

The shared component model has gained popularity among the joint disease mapping concepts. The addition of the temporal component to exclusively spatial models is another development that strengthens the inference of disease data. However, most of the research in the field of disease mapping studies focused on the spatial or temporal modeling of a specific disease and was conducted at the univariate level [13]. Despite the advantages of the separated approach, it cannot account for the possible association between the two diseases together. A combined

model of typhoid and malaria is needed to explore the interaction between the two diseases and identify variables associated with both [14].

Certain diseases have comparable risk factors, as previously mentioned. The emerging trend in multivariate disease mapping, which is the combined modeling of the spatial occurrence of two or more diseases or health outcomes, may have its roots in a lack of motivation to incorporate data from related diseases. When we employ this method as opposed to examining each situation separately, we may anticipate having access to more information. Benefits from this include the capacity to draw attention to both typical and distinctive geographical patterns of the various diseases [13].

By adding time and space-time interaction to the previously only spatial models, disease mapping has been improved. Since the ability to examine and detect the persistence or systematic evolution of geographical patterns over time gives more compelling evidence of genuine differences than a single cross-sectional analysis, these analyses are far more advantageous than the merely spatial disease mapping. In this work we shall create a joint disease mapping model that combines the concept of multivariate shared components with spatio-temporal modeling. In order to achieve this, the shared components in the suggested model take temporal and spatial aspects into account [13].

The existing literature for spatial and spatio-temporal dynamics of disease co-infections basically focused on the co-infection between malaria and anaemia [14], HIV and TB [15], malaria, dengue and chikungunya [16], [17]. However, in deterministic modelling malaria and typhoid co-infection was given an attention as in the research by [6].

In their mathematical (compartmental) model [4] presented illustrative numerical results with a case study in the Eastern Province of Kenya to quantify the possible false diagnosis resulting from this co-infection. Although malaria is more problematic in terms of new infections and diseased deaths in Kenya, they found that false diagnosis with higher possible cases for typhoid than malaria causes significant devastating impacts on Kenyan societies. Their results showed that both diseases needed to be managed simultaneously for successful control of co-epidemics.

Currently, the most widely used Bayesian technique for obtaining posterior inference, particularly in complex statistical models, is the Markov chain Monte Carlo(MCMC) method. It is

acknowledged, yet, that MCMC techniques frequently entail a lengthy processing time, convergence difficulties, and poor scalability when applied to high-dimensional spatio-temporal disease models [18]. Faster samplers are required as a statistical modeler has to be able to quickly switch between models. In order to directly calculate precise approximations to the posterior marginal distributions, a proposal to use an integrated nested Laplace approximation(INLA) that seems to be quicker than MCMC was suggested by [19].

Although interest in infectious disease modeling has increased, previous research on malaria and typhoid has mainly treated the two diseases independently and has not jointly examined the impact of climatic conditions and their combined spatial and temporal structures on co-infection patterns [4], [20]. Consequently, the effects of environmental drivers such as temperature, precipitation, and humidity on the concurrent spread and persistence of both diseases in regions where they co-exist are not well characterized. To overcome this limitation, this study proposes a Bayesian hierarchical spatio-temporal framework for the joint modeling of malaria–typhoid co-infection, incorporating both common and disease specific spatial and temporal components influenced by climatic variables.

Based on simulated datasets and inference using INLA, the study investigates key statistical properties of the resulting parameter estimates, including bias, consistency, asymptotic normality, and efficiency.

The rest of the paper is organized as follows: Section 2 is about mathematical model derivation and formulation, Section 3 is about simulation, Section 4 contains discussion while Section 5 draws conclusion.

2. Mathematical Model Derivation and Formulation

2.1. Model development.

The central idea of the Bayesian approach is to combine the likelihood with your prior knowledge (prior probability) to result in a revised probability (posterior probability) [21].

We assumed that the outcome $Y_{it}|\delta_{it} \sim \text{Binomial}(n_{it}, \pi_{it})$ and the spatio-temporal process was defined on the linear predictor δ_{it} by the link function in Equation (2.1). The binary Y_{it} has two outcomes 1 and 0, 1 means that the tested individual was positive for both diseases contrarily 0 stands for an individual tested and confirmed either one disease or none of them.

$$\delta_{it} = \beta_0 + {X_{it}}^T \beta + u_i + v_i + \gamma_t + \tau_t + \alpha_{it} \tag{2.1}$$

with β_0 the intercept, β vector regression coefficient for K covariates, denoted as $X_{it} = (X_{1it}, \ldots, X_{kit})$, u_i structured spatial effects, v_i unstructured spatial effects, γ_t structured temporal effects, τ_t unstructured temporal effects and α_{it} interaction between space and time.

2.1.1. *The likelihood function.*

The likelihood function is a function of the model parameters, defined as the probability of the observed data viewed as a function of those parameters [22]. From Equation (2.1) the likelihood function is derivered as in Equation (2.2) and (2.4):

$$\mathscr{L}_y = \prod_{i=1}^{N}\prod_{t=1}^{T} \binom{n_{it}}{y_{it}} \pi_{it}^{y_{it}} (1-\pi_{it})^{n_{it}-y_{it}} \tag{2.2}$$

In Equation (2.2) N is the number of spatial units and T are time points with a range of indices: $i = 1, \ldots, N; t = 1, \ldots, T$. Thus, the likelihood is computed over $N \times T$ observations. The probability of success in Equation (2.2) is given as below:

$$\pi = \frac{\exp(\delta_{it})}{1+\exp(\delta_{it})} \tag{2.3}$$

Therefore, the likelihood becomes:

$$\mathscr{L}(y|\theta) = \prod_{i=1}^{N}\prod_{t=1}^{T} \binom{n_{it}}{y_{it}} \frac{\left(\exp\left(\beta_0 + X_{it}^T\beta + u_i + v_i + \gamma_t + \tau_t + \alpha_{it}\right)\right)^{y_{it}}}{\left(1+\exp\left(\beta_0 + X_{it}^T\beta + u_i + v_i + \gamma_t + \tau_t + \alpha_{it}\right)\right)^{n_{it}}} \tag{2.4}$$

2.1.2. *Priors.*

A prior is a probability distribution that represents beliefs or knowledge about a parameter before observing any data. The model in Equation (2.1) has below assumptions for priors:

According to [23] the spatially structured prior was assumed to follow an Intrinsic Conditional Autoregressive(ICAR) , $u_i \mid u_{j\neq i} \sim \mathscr{N}\left(\frac{\sum_{j\neq i} w_{ij}u_j}{\sum_{j\neq i} w_{ij}}, \frac{\sigma_u^2}{\sum_{j\neq i} w_{ij}}\right)$ with w_{ij} represents the first-order adjacency weights matrix, where $w_{ij} = 1$ if areas i and j share boundaries and $w_{ij} = 0$ otherwise. On the other hand, the unstructured spatial effect $v_i \sim \mathscr{N}(0, \sigma_v^2)$ [1] .

The structured temporal effect γ_t is modeled dynamically as stationary Autoregressive(AR) [24]:

i. Stationary AR(1)

$$\gamma_t | \gamma_{t-1} \sim \mathscr{N}\left(0, \frac{\sigma^2}{1-\phi_1^2}\right), \tag{2.5}$$

with $|\phi_1| < 1$ and $\phi_1 \sim \mathscr{U}(0,1)$, alternatively,

ii. Stationary AR(2)

$$\gamma_t|\gamma_{t-1},\gamma_{t-2} \sim \mathscr{N}\left(0, \frac{\sigma^2}{1-\phi_1^2-\phi_2^2-2\phi_1\phi_2}\right) \tag{2.6}$$

In turn, the temporal unstructured effect τ_t is specified by means of a Gaussian exchangeable prior, $\tau_t \sim \mathscr{N}(0, \frac{1}{\varepsilon_\tau})$ [18].

The interaction term between space and time $\alpha = (\alpha_{it})$ is modeled as a multivariate normal vector [18]:

$$\alpha \sim \mathscr{N}\left(0, (\varepsilon_\alpha R_\alpha)^{-1}\right)$$

Hence, the structure matrix of α is defined using the Kronecker product:

$$R_\alpha = R_u \otimes R_\gamma$$

With R_u the $N \times N$ spatial structure matrix (e.g., from ICAR prior), R_γ is the $T \times T$ temporal structure matrix (e.g., AR(1) or AR(2)), $\otimes$ denotes the Kronecker product.

The precision matrix is obtained from Equation (2.7):

$$Q = D - W \tag{2.7}$$

The diagonal matrix of neighborhood degrees D is computed as:

$$D = \text{diag}(d_1, d_2, \ldots, d_N), \quad \text{where} \quad d_i = \sum_{j=1}^{N} w_{ij}.$$

That is, D_{ii} equals the number of neighbors of region i. This formulation assumes Type IV interaction (structured space × structured time) as shown in Table 1, capturing dependencies across both space and time with vector α of length $N \times T$.

For the four interaction components, the priors are the products of the priors of the corresponding components.

2.1.3. *The posterior distribution.*

The posterior distribution is the probability distribution of an unknown parameter after observing the data [21], it combines the prior and the likelihood as in Equation (2.8):

$$P(\theta|y) = \frac{\mathscr{L}(y|\theta)P(\theta)}{P(y)} \tag{2.8}$$

TABLE 1. Summary of types of interaction

Interaction	Parameter interacting
I	v_i and τ_t
II	γ_t and v_i
III	u_i and τ_t
IV	u_i and γ_t

From Equation (2.8), the normalizing constant is given by:

$$P(y) = \int_{\theta} \left[\prod_{i=1}^{N} \prod_{t=1}^{T} \binom{n_{it}}{y_{it}} \cdot \frac{(\exp(\delta_{it}))^{y_{it}}}{(1+\exp(\delta_{it}))^{n_{it}}} \right] \cdot P(\theta)\, d\theta \tag{2.9}$$

with $P(\theta) = \prod_{h \in \theta} P(h)$ and $\theta = (\beta, u, v, \gamma, \tau, \alpha, \sigma_u^2, \sigma_v^2, \sigma_\gamma^2, \sigma_\tau^2, \sigma_\alpha^2)$.

2.2. Bayesian hierarchical model.

A Bayesian Hierarchical Model (BHM) is a Bayesian statistical model that is built in layers (levels), where each level describes different sources of variability or uncertainty [21]. The developed spatio-temporal model is classified into the following hierarchies:

- Level 1: Data (Likelihood)

$$\begin{cases} Y_{it} | \delta_{ij} \sim \text{Binomial}\left(n_{it}, \pi_{it}\right), \pi = \dfrac{\exp(\delta_{it})}{1+\exp(\delta_{it})} \\ \delta_{it} = \beta_0 + {X_{it}}^T \beta + u_i + v_i + \gamma_t + \tau_t + \alpha_{it} \end{cases}$$

- Level 2: Latent Effects

$$\begin{cases} u_i \sim CAR(\sigma_u^2) \\ v_i \sim \mathcal{N}(0, \sigma_v^2) \\ \tau_t \sim \mathcal{N}(0, \varepsilon_\tau^{-1}) \\ \gamma_t | \gamma_{t-1} \sim \mathcal{N}\left(0, \sigma^2 \left[1-\phi_1^2\right]^{-1}\right), \phi_1 \sim \mathscr{U}(0,1) \\ \alpha_{it} \sim \mathcal{N}\left(0, \sigma_\alpha^2 \left[\mathbf{R}_v \otimes \mathbf{R}_\tau\right]^{-1}\right) \end{cases}$$

- Level 3: Hyperpriors: To complete the Bayesian hierarchy, we place hyperpriors on the variance parameters using an Inverse-Gamma prior $\sigma_k^{-2} \sim \text{Gamma}(a_k, b_k)$, for $k \in$

$\{\beta, u, v, \gamma, \tau, \alpha\}$, Where a_k and b_k are hyperparameters controlling the prior distribution of variances.

The hierarchical model is illustrated by Figure 1:

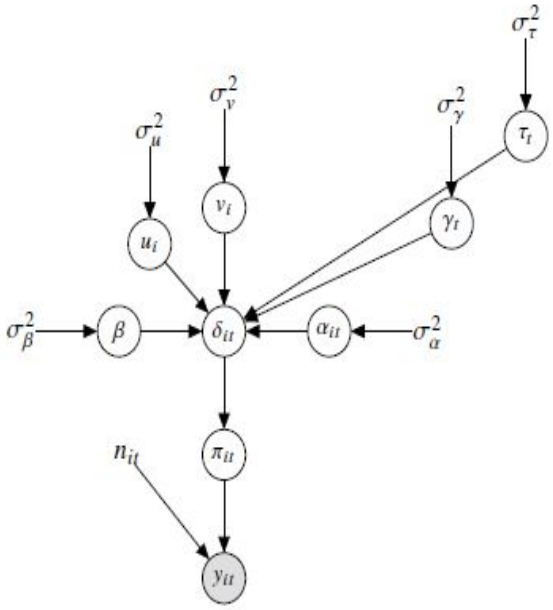

Figure 1. Hierarchical Model Representation

2.3. Parameter Estimation.

2.3.1. *Joint posterior distribution.*

As it was started in Section 1 an alternative approach to the simulation based MC integration is analytic approximation with the Laplace method [19]. The joint posterior distribution of δ and θ is given by the product of the likelihood of the Gaussian Markov Random Field(GMF) density and of the hyperparameter prior distribution.

$$\begin{aligned} P(\delta,\theta|y) &\propto p(\theta)\times p(\delta|\theta)\times p(y|\delta,\theta) \\ &\propto p(\theta)\times p(\delta|\theta)\times\prod_{i=1}^{N}\prod_{t=1}^{T}p(y_{it}|\delta_{it},\theta) \\ &\propto p(\theta)\times|Q(\theta)|^{\frac{1}{2}}\exp\left(-\frac{1}{2}\delta' Q^{-1}(\theta)\delta\right)\times\prod_{i=1}^{N}\prod_{t=1}^{T}\exp\left(\log(p(y_{it}|\delta_{it},\theta))\right) \\ &\propto p(\theta)\times|Q(\theta)|^{\frac{1}{2}}\exp\left(-\frac{1}{2}\delta' Q^{-1}(\theta)\delta+\sum_{i}^{N}\sum_{t=1}^{T}\log(p(y_{it}|\delta_{it},\theta))\right) \end{aligned} \tag{2.10}$$

2.3.2. *The marginal posterior.*

The marginal posterior of each latent field component δ_i is computed using:

$$\begin{aligned} p(\delta_i|y) &= \int p(\delta_i,\theta|y)d\theta \\ &= \int p(\delta_i|\theta,y)p(\theta|y)d\theta \end{aligned} \tag{2.11}$$

and for each element of the hyperparameter vector, we obtain that:

$$p(\theta_i|y) = \int p(\theta|y)d\theta_{-i} \tag{2.12}$$

where θ_{-i} represents the vector θ without the element θ_i.

The main task consists of the computation of an approximation to the joint posterior of the hyperparameters. We therefore, approximate $p(\delta_i|\theta,y)$ and $p(\theta|y)$ as in Equations (2.13), (2.14):

$$\begin{aligned} p(\theta \mid \mathbf{y}) &= \frac{p(\delta,\theta \mid \mathbf{y})}{p(\delta \mid \theta,\mathbf{y})} \\ &= \frac{p(\theta)\times p(\delta \mid \theta)\times p(\mathbf{y} \mid \delta,\theta)}{p(\mathbf{y})}\cdot\frac{1}{p(\delta \mid \theta,\mathbf{y})} \\ &\propto \frac{p(\theta)\times p(\delta \mid \theta)\times p(\mathbf{y} \mid \delta,\theta)}{p(\delta \mid \theta,\mathbf{y})} \\ &\approx \left.\frac{p(\theta)\times p(\delta \mid \theta)\times p(\mathbf{y} \mid \delta,\theta)}{\tilde{p}(\delta \mid \theta,\mathbf{y})}\right|_{\delta=\delta^*(\theta)} =: \tilde{p}(\theta \mid \mathbf{y}) \end{aligned} \tag{2.13}$$

where $\tilde{p}(\delta \mid \theta,\mathbf{y})$ is the Gaussian approximation (via the Laplace method) to $p(\delta \mid \theta,\mathbf{y})$, and $\delta^*(\theta)$ is the mode for a given θ.

$$\begin{aligned} p(\delta_i|\theta,y) &= \frac{p((\delta_i,\delta_{-i})|\theta,y)}{p(\delta_{-i}|\delta_i,\theta,y)} \\ &= \frac{p(\delta,\theta|y)}{p(\theta|y)}\frac{1}{p(\delta_{-i}|\delta_i,\theta,y)} \\ &\propto \frac{p(\delta,\theta|y)}{p(\delta_{-i}|\delta_i,\theta,y)} \\ &\approx \left.\frac{p(\delta,\theta|y)}{\tilde{p}(\delta_{-i}|\delta_i,\theta,y)}\right|_{\delta_{-i}=\delta^*_{-i}(\delta_i,\theta)} =: \tilde{p}(\delta_i|\theta,y) \end{aligned} \tag{2.14}$$

As mentioned in Equation (2.12) δ_{-i} indicates the vector δ without the i^{th} element.

2.4. Properties of parameter estimators.

2.4.1. *Unbiasedness.*

The Bayesian estimate of θ is:

$$\begin{aligned}\hat{\theta} = \mathbb{E}[\theta \mid Y] &= \int_{\theta} \theta P(\theta \mid Y) d\theta \\ &= \int_{\theta} \theta \frac{\mathscr{L}(y|\theta)P(\theta)}{P(y)} d\theta\end{aligned} \tag{2.15}$$

Since this integral can not be analytically obtained, we use INLA to approximate [25]:

$$\hat{\theta} \approx \sum_{k} \theta_k w_k, \tag{2.16}$$

where θ_k are posterior samples and w_k are posterior weights.

The posterior weights are given by:

$$w_k = \frac{P(y|\theta_k)P(\theta_k)}{\sum_{j=1}^{K} P(y|\theta_j)P(\theta_j)}. \tag{2.17}$$

Unbiasedness in a Bayesian sense means $\mathbb{E}_{\theta|Y}[\hat{\theta}] = \theta$ that is the expected value of the INLA estimator is the true value.

2.4.2. *Consistency.*

As the number of observations $N \times T \to \infty$, the posterior concentrates around the true parameter values. The consistency is determined using Equation (2.18) as shown by [26]:

$$\lim_{N,T\to\infty} \mathbb{P}\left(\|\theta - \hat{\theta}\| > \varepsilon \mid y\right) = 0, \tag{2.18}$$

with ε the tolerance level. Alternatively, the posterior mean $\mathbb{E}(\theta \mid y)$ is consistent if:

$$\lim_{N,T\to\infty} \mathbb{E}(\hat{\theta} \mid y) = \theta \tag{2.19}$$

The Equation (2.19) tells us that an estimator is said to be consistent if its probability limit is equal to the true value of the parameter in question.

2.4.3. *Asymptotic normality/Asymptotic efficient.*

In GLMM / Bayesian spatio-temporal models:

i. Many fixed effect estimators (e.g., climatic covariates) become approximately normal as the number of spatial locations or time points increases.

ii. In Bayesian models, the posterior distribution of parameters becomes approximately Gaussian (Laplace approximation used by INLA relies on this!).

iii. However, asymptotic normality does not guarantee that the estimator is optimal, it only means that it becomes normally distributed.

An estimator is asymptotically normal if the posterior distribution of each parameter tends toward a normal distribution centered at the true value as the sample size increases.:

$$\sqrt{NT}\left(\theta-\hat{\theta}\right) \xrightarrow{d} \mathcal{N}(0,\Sigma)$$

The posterior distribution becomes asymptotically efficient when it achieves the minimum possible variance allowed by the Cramér–Rao lower bound (CRLB)., as was shown by [27], [28]:

$$\sqrt{NT}\left(\theta-\hat{\theta}\right) \xrightarrow{d} \mathcal{N}\left(0,I^{-1}(\hat{\theta})\right)$$

where $I(\theta_0)$ is the Fisher Information matrix.
The (asymptotic) Cramér–Rao lower bound (matrix) for $\hat{\theta}$ is:

$$\text{Var}(\hat{\theta}) \succeq \frac{1}{NT} I^{-1}(\theta).$$

Some of spatial/random effects may not be asymptotically efficient due to: shrinkage (from priors), spatial/temporal dependence, penalized complexity (PC) priors, among others.

3. SIMULATION

3.1. Background of the simulation.

A simulation study is performed in this work to analyze the influences of climatic factors on the spatio-temporal patterns of malaria-typhoid co-infection. According to the complexity of this article only three parameters were considered, these are temperature, precipitation and humidity. The data set was simulated under the proposed model respecting the distributions assumed under the Bayesian hierarchies. We chose 20 spatial units and 72 time points resulting in 1,440 observations. Each location was assumed to have four neighbors i.e four cardinal points.

The binary dependent variable Y_{it} is generated based on the specifications of a comprehensive spatio-temporal model structure. Mainly we focused on the structured spatial and structured temporal interactions (type IV) as shown in Table 1. This choice is made due to the general understanding that the spatial and temporal variation in disease risk is primarily influenced by

its spatio-temporal dependencies. Moreover, we were curious to know what happens if the spatial and temporal dependencies were ignored. Thus, considering Equation (2.1) we dropped out the interactions and simulated again in order to compare the two models.

3.2. Results.

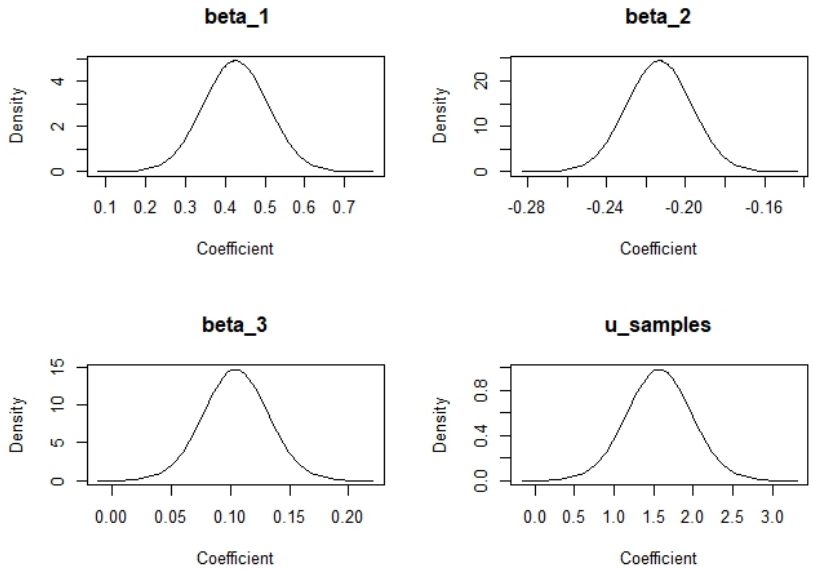

Figure 2. β_1, β_2, β_3 and u

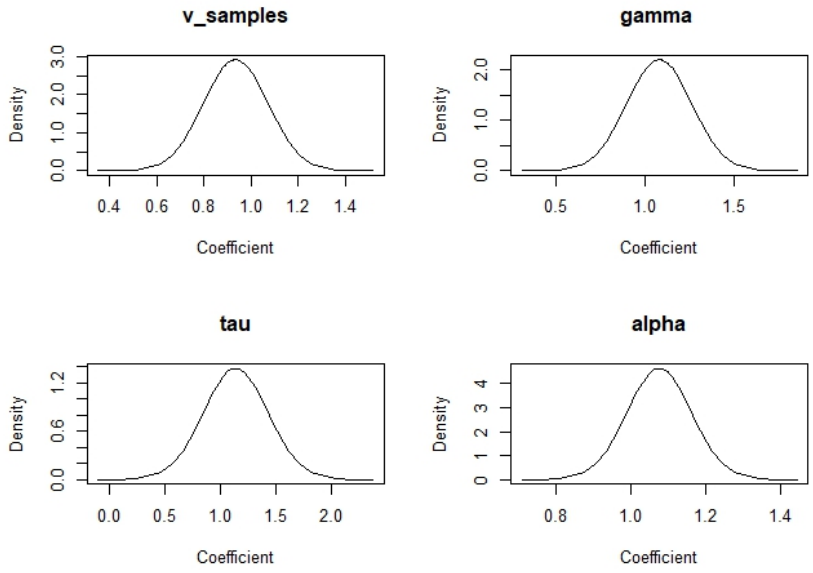

Figure 3. v,γ , τ and α

The kernel densities for the marginal posteriors in Figure 2 and 3 are bell curved shapes i.e normally distributed. The posterior mean, median, and mode of the parameter estimates were identical, indicating a symmetric and unimodal posterior distribution and suggesting asymptotic normality of the estimators as shown in Table 2. Since kernel density plots alerts a smooth empirical histogram and warns that the distribution of parameters is normal a good mixing of the samples is noticed.

TABLE 2. Statistics of fixed and random effects

Effects:							
	Estimates	std	0.025quant	0.5quant	0.975quant	mode	kld
Intercept (β_0)	0.4772164	2.18550885	-3.80630225	0.4772164	4.7607350	0.4772164	0
Temperature (β_1)	0.4256132	0.08097513	0.26690487	0.4256132	0.5843215	0.4256132	0
Precipitation (β_2)	-0.2132314	0.01631786	-0.24521377	-0.2132314	-0.1812490	-0.2132314	0
Humidity (β_3)	0.1040561	0.02725229	0.05064257	0.1040561	0.1574696	0.1040561	0
u	1.5726047	0.40584499	0.77716313	1.5726047	2.3680462	1.5726047	0
v	0.9328627	0.13649756	0.66533238	0.9328627	1.2003930	0.9328627	0
γ	1.0797150	0.18048400	0.72597289	1.0797150	1.4334572	1.0797150	0
τ	1.1344442	0.28920167	0.56761935	1.1344442	1.7012691	1.1344442	0
α	1.0770763	0.08622076	0.90808670	1.0770763	1.2460658	1.0770763	0
DIC: 359.91							
DIC, saturated: 357.82							
WAIC: 360.27							

From Table 2 we realized that the temperature has a high impact on the co-infection than other variables while lower precipitation is associated with increased risk. The structured spatial effect u estimate which is equal to 1.5726047 revealed a bigger influence on the the disease co-infection than other spatial and temporal components.

TABLE 3. Bias agains Standard Deviation and RMSE

Effects	N	Bias	SD	RMSE
Temperature	100	3.467876	2.422445151	4.230178019
Precipitation	100	-1.136298	0.796752597	1.387800030
Humidity	100	0.3060903	0.339255904	0.456930889
Temperature	500	0.1790526	0.133358603	0.223258486
Precipitation	500	-0.01598942	0.026161685	0.030660972
Humidity	500	0.01350985	0.050756990	0.052524167
Temperature	1,000	0.001750979	0.027886171	0.032927666
Precipitation	1,000	-0.006647164	0.005941810	0.008915711
Humidity	1,000	0.007186352	0.010513623	0.012734988
Temperature	10,000	-0.009259673	0.008606619	0.012641813
Precipitation	10,000	-0.000310426	0.001817906	0.001818171
Humidity	10,000	-0.008792766	0.003262901	0.009378659

As it is shown in Table 3 when the sample size increases the bias, standard deviation and the root mean squared errors decrease. This confirms to us that the estimator is unbiased it means for bigger sample sizes the estimate is approximately equal to the true value. The unbiasedness property is assured by the Figure 4, 5 and 6.

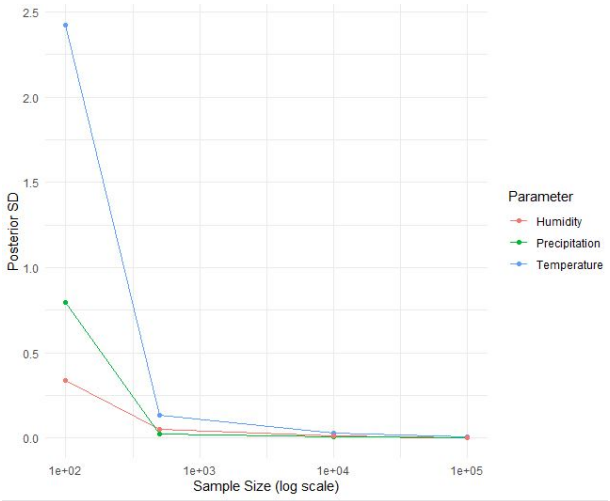

Figure 4. Posterior standard deviation versus sample size

Referring to Figure 4 the posterior SD decreases sharply as sample size increases. Thus, the flat curves beyond 1000 observations means that the sample size is sufficient and the estimator

is consistent. Table 3 tells us that the posterior distribution is asymptotically efficient since its variance critically reduced approaching 0 as the sample size increases.

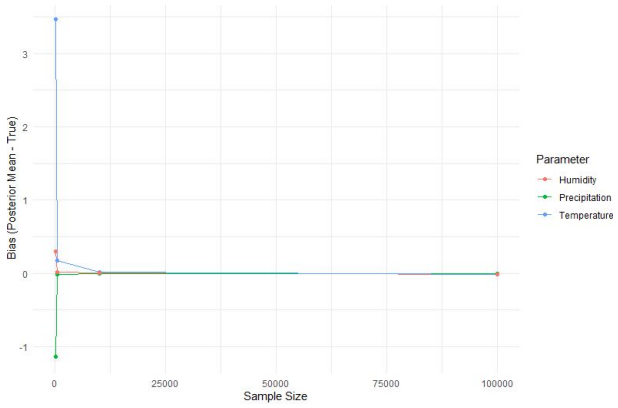

Figure 5. Bias versus sample size

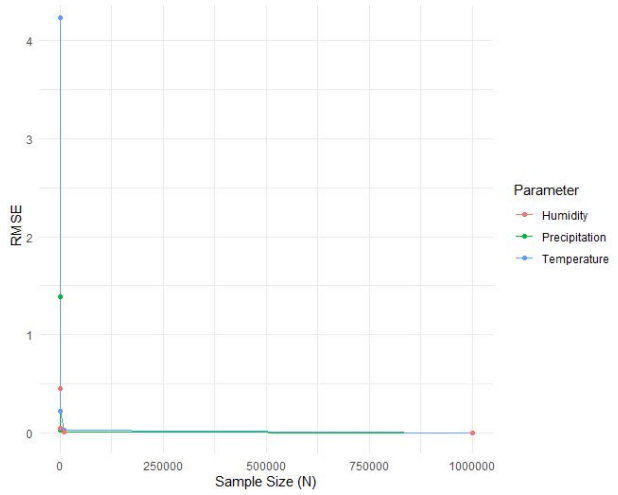

Figure 6. RMSE versus sample size

To verify consistency as the sample size increases, we relied on asymptotic normality and a shrinking variance. According to the information displayed by Figure 3 and 4 we noticed that the more N raises the mean z tends to 0, the standard deviation is close to 1. Therefore,the asymptotic normality property of the estimation is assured .

TABLE 4. Asymptotic Normality Metrics Across Sample Sizes

N	Parameter	Mean Z	SD Z	Skewness	Kurtosis	Shapiro-p	KS-p
100	β_0	0.097004672	0.9846768	0.09682802	-0.642445073	0.35385459	0.5357963
	β_1	-0.062417245	0.9796954	-0.34623377	0.156961179	0.06461233	0.7979909
	β_2	-0.001951446	0.9625035	-0.26552623	-0.829934747	0.42859881	0.7979909
	β_3	0.039918166	0.9144956	0.15399999	-0.120427009	0.86177050	0.7538692
500	β_0	0.01374929	0.9737056	-0.231239253	-0.08438697	0.1066643	0.5386957
	β_1	-0.02900503	0.9843478	0.017108186	0.01617626	0.8295488	0.7330014
	β_2	-0.07465640	0.9707805	-0.040493731	-0.10985945	0.8757110	0.3758339
	β_3	0.01411593	0.9554351	-0.002484899	-0.10148770	0.8917519	0.8903220
1000	β_0	-0.026077760	0.9855316	0.10159488	0.073374823	0.76409042	0.2415974
	β_1	-0.052975973	0.9926400	0.02703901	0.125049526	0.26124101	0.1494841
	β_2	-0.015085499	0.9626027	0.12545025	-0.117679795	0.23900996	0.3543863
	β_3	0.022505819	0.9874609	0.16441206	0.196912249	0.09781540	0.8368466
5000	β_0	-0.007490971	1.0025135	0.01457699	-0.011561255	0.3319473	0.97393031
	β_1	-0.046007789	1.0086302	-0.03205900	0.084853344	0.3047146	0.01217122
	β_2	0.007918859	1.0006868	0.06004791	-0.053836013	0.1741572	0.86101451
	β_3	-0.009707735	0.9854088	0.01464076	-0.099236834	0.1333701	0.62880544

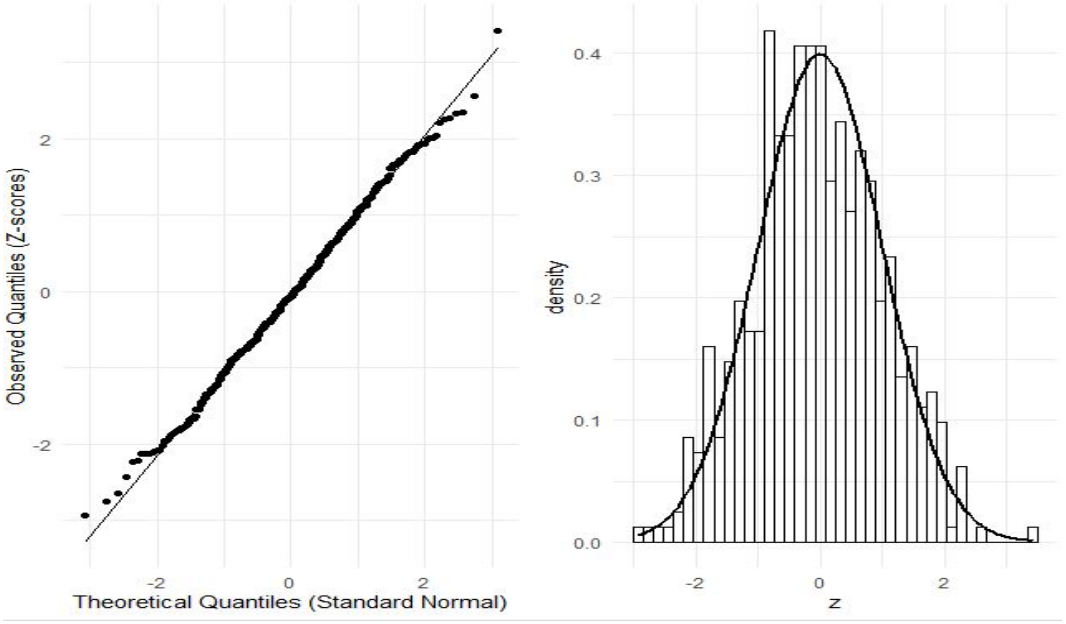

Figure 7. QQ Plot and Histogram for N=100

The QQ-plots and histograms of the standardized estimator in Figure 7 and 8 show close agreement with the standard normal distribution, providing strong empirical evidence of asymptotic normality; the increasing concentration and unit variance behavior further indicate that the estimator is asymptotically efficient.

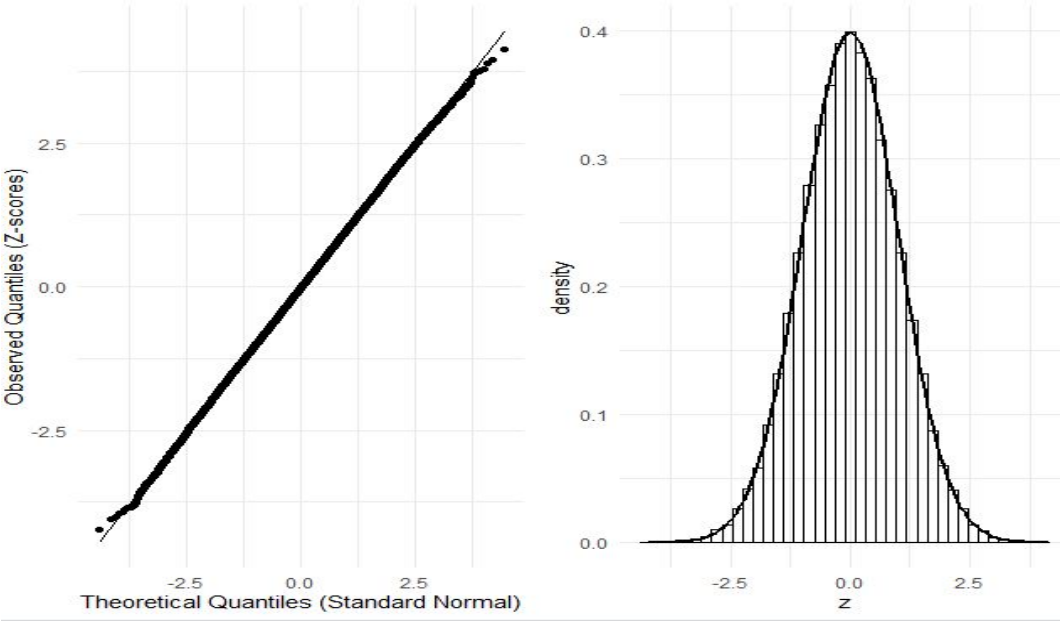

Figure 8. QQ Plot and Histogram for N=100,000

Above cited figures witness that the asymptotic normality is perfectly guaranteed for bigger sample sizes e.g N=100,000. Whereas, for small sample size N=100 a slight deviation from standard normal was observed.

4. Discussion

Malaria and typhoid co-infection was ignored for a long period of time. Nevertheless, it is a real probable situation. Estimating separate time trends for each area is inefficient due to complex spatial–temporal dependence and high variability in chronic outcomes. A Bayesian hierarchical model improves inference by borrowing strength across space and time to identify common patterns while allowing heterogeneity. A joint mixture model for space–time interactions, combined with well chosen priors, ensures identifiability and enables clear separation between minor fluctuations and truly significant interactions.

Our results confirmed relationships found in the West Nile Virus modeling (WNV) literature with respect to temperature and precipitation in the eastern United States by [24], in which higher temperature and lower precipitation were associated with increased WNV incidence as in Table 2. On another hand for [29] the most influential component in explaining dengue risk in West Java was the spatially structured effects which is consistent with the outputs shown in Table 2. Even though, precipitation in this manuscript claimed a negative correlation this contradicts the outputs from [30] that confirmed a positive correlation among other reasons should be due to local seasonal patterns. The findings in this work agree with [31] that once interaction of type IV as in Table 1 is added in the model we observe an overparameterization and hence could lead to a loss of precision. The marginal posteriors in Figure 2 and 3 go along with the results from [32] showing that the parameters fitted well as GMRF since they are symmetrical about thus the mean equals the median and mode.

5. CONCLUSION

The aim of this paper was to examine the properties of the estimators for fixed and random effects in a Bayesian spatio-temporal model with climatic factor covariates. The considered independent variables were temperature, precipitation and humidity. As earlier discussed, we conducted a simulation study that generated a total of 1,440 observations.

In order to account for variance not accounted for by the fixed effects, our model looked at the spatial and temporal dynamics of the disease co-infection. The limited non-spatiotemporal model and the complete model are compared, both the DIC and WAIC demonstrated that adding the temporal and spatial effects led to a better model fit. Hovewer, as forediscussed introducing space–time interaction unnecessarily overparameterizes the model i.e the lack of parsimony . It is fortunate to claim that the estimator in our model was unbiased, asymptotically normal, asymptotically efficient and consistent as it was discussed in Figure 4, 6, 7 and 8 as well as in Table 3 and 4. Since the properties of the estimators were preserved, we can trust the developed model to be applied on malaria-typhoid co-infection real data.

Despite that the model is trusted for real data set application, we encountered challenges and limitations in this article. For instance, we did not include in our model variables such as interventions strategies, environmental , geographical and socio-demographic. Moreover,

they was an obstacle to obtain the co-infection real data because there are not health policy to diagnose them simultaneous. Therefore, we recommend future work to account for the these non-considered factors.

CONFLICT OF INTERESTS

The authors declare that there is no conflict of interests.

REFERENCES

[1] J.M.K. Aheto, L.J. Menezes, W. Takramah, L. Cui, Modelling Spatiotemporal Variation in Under-Five Malaria Risk in Ghana in 2016–2021, Malar. J. 23 (2024), 102. https://doi.org/10.1186/s12936-024-04918-x.

[2] S.D. Vasava, S.J. Lakhani, J.D. Lakhani, Prevalence of malaria and typhoid fever and coinfection in all febrile patients attending at tertiary care hospital in Vadodara, J. Appl. Biol. Biotech. 9 (2021), 136–140. https://doi.org/10.7324/JABB.2021.9518.

[3] J.D. Nzabakiriraho, E. Gayawan, Geostatistical Modeling of Malaria Prevalence among Under-Five Children in Rwanda, BMC Public Health 21 (2021), 369. https://doi.org/10.1186/s12889-021-10305-x.

[4] J.M. Mutua, F.B. Wang, N.K. Vaidya, Modeling Malaria and Typhoid Fever Co-Infection Dynamics, Math. Biosci. 264 (2015), 128–144. https://doi.org/10.1016/j.mbs.2015.03.014.

[5] M. Birhanie, B. Tessema, G. Ferede, M. Endris, B. Enawgaw, Malaria, Typhoid Fever, and Their Coinfection among Febrile Patients at a Rural Health Center in Northwest Ethiopia: A Cross-Sectional Study, Adv. Med. 2014 (2014), 531074. https://doi.org/10.1155/2014/531074.

[6] Z.A. Workie, P.R. Koya, Mathematical Modelling of the Co-Infection Dynamics of Typhoid Fever with Plasmodium Vivax and Plasmodium Falciparum with Treatment, Math. Model. Appl. 7 (2022), 1–25.

[7] A.Y. Liu, J.M. Trtanj, E.K. Lipp, J.M. Balbus, Toward an Integrated System of Climate Change and Human Health Indicators: A Conceptual Framework, Clim. Chang. 166 (2021), 49. https://doi.org/10.1007/s10584-021-03125-w.

[8] J.J. Cheng, P. Berry, Development of Key Indicators to Quantify the Health Impacts of Climate Change on Canadians, Int. J. Public Health 58 (2013), 765–775. https://doi.org/10.1007/s00038-013-0499-5.

[9] X. Wu, Y. Lu, S. Zhou, L. Chen, B. Xu, Impact of Climate Change on Human Infectious Diseases: Empirical Evidence and Human Adaptation, Environ. Int. 86 (2016), 14–23. https://doi.org/10.1016/j.envint.2015.09.007.

[10] J.U. Ibeji, H. Mwambi, A.K. Iddrisu, Bayesian Spatio-Temporal Modelling and Mapping of Malaria and Anaemia among Children Between 0 and 59 Months in Nigeria, Malar. J. 21 (2022), 311. https://doi.org/10.1186/s12936-022-04319-y.

[11] Q. Gao, Z. Liu, J. Xiang, Y. Zhang, M.X. Tong, et al., Impact of Temperature and Rainfall on Typhoid/Paratyphoid Fever in Taizhou, China: Effect Estimation and Vulnerable Group Identification, Am. J. Trop. Med. Hyg. 106 (2022), 532–542. https://doi.org/10.4269/ajtmh.20-1457.

[12] M. Masjkur, H. Folmer, Bayesian Estimation of Spatio-Temporal Models with Covariates Measured with Spatio-Temporally Correlated Errors: Evidence from Monte Carlo Simulation, in: Proceedings of the 4th Bandung Creative Movement International Conference on Creative Industries 2017 (4th BCM 2017), Atlantis Press, Paris, France, 2018. https://doi.org/10.2991/bcm-17.2018.61.

[13] B. Mahaki, Y. Mehrabi, A. Kavousi, V.J. Schmid, Joint Spatio-Temporal Shared Component Model with an Application in Iran Cancer Data, Asian Pac. J. Cancer Prev. 19 (2018), 1553. https://doi.org/10.22034/APJCP.2018.19.6.1553.

[14] R.T. Gaston, S. Ramroop, F. Habyarimana, Joint Modelling of Malaria and Anaemia in Children Less Than Five Years of Age in Malawi, Heliyon 7 (2021), e06899. https://doi.org/10.1016/j.heliyon.2021.e06899.

[15] V. Otiende, T. Achia, H. Mwambi, Bayesian Modeling of Spatiotemporal Patterns of Tb-HIV Co-Infection Risk in Kenya, BMC Infect. Dis. 19 (2019), 902. https://doi.org/10.1186/s12879-019-4540-z.

[16] N. Salam, S. Mustafa, A. Hafiz, A.A. Chaudhary, F. Deeba, et al., Global Prevalence and Distribution of Coinfection of Malaria, Dengue and Chikungunya: A Systematic Review, BMC Public Health 18 (2018), 710. https://doi.org/10.1186/s12889-018-5626-z.

[17] W. Mala, P. Wilairatana, K.U. Kotepui, M. Kotepui, Prevalence of Malaria and Chikungunya Co-Infection in Febrile Patients: A Systematic Review and Meta-Analysis, Trop. Med. Infect. Dis. 6 (2021), 119. https://doi.org/10.3390/tropicalmed6030119.

[18] M. Blangiardo, M. Cameletti, Spatial and Spatio-temporal Bayesian Models with R-INLA, Wiley, 2015. https://doi.org/10.1002/9781118950203.

[19] F. Lindgren, H. Rue, Bayesian Spatial Modelling with R-INLA, J. Stat. Softw. 63 (2015), 1–25. https://doi.org/10.18637/jss.v063.i19.

[20] T.O. Ogunlade, O.M. Ogunmiloro, G.E. Fatoyinbo, On the Deterministic and Stochastic Model Applications to Typhoid Fever Disease Dynamics, J. Phys.: Conf. Ser. 1734 (2021), 012048. https://doi.org/10.1088/1742-6596/1734/1/012048.

[21] E. Lesaffre, A.B. Lawson, Bayesian Biostatistics, Wiley, 2012. https://doi.org/10.1002/9781119942412.

[22] G.E. Box, G.C. Tiao, Bayesian Inference in Statistical Analysis, Wiley, 2011. https://doi.org/10.1002/9781118033197.

[23] L. Knorr-Held, J. Besag, Modelling Risk from a Disease in Time and Space, Stat. Med. 17 (1998), 2045–2060. https://doi.org/10.1002/(sici)1097-0258(19980930)17:18⟨2045::aid-sim943⟩3.0.co;2-p.

[24] M.H. Myer, J.M. Johnston, Spatiotemporal Bayesian Modeling of West Nile Virus: Identifying Risk of Infection in Mosquitoes with Local-Scale Predictors, Sci. Total. Environ. 650 (2019), 2818–2829. https://doi.org/10.1016/j.scitotenv.2018.09.397.

[25] A. Gelman, J.B. Carlin, H.S. Stern, D.B. Rubin, Bayesian Data Analysis, Chapman and Hall/CRC, 1995. https://doi.org/10.1201/9780429258411.

[26] T. Maitra, S. Bhattacharya, On Classical and Bayesian Asymptotics in Stochastic Differential Equations with Random Effects Having Mixture Normal Distributions, J. Stat. Plan. Inference 208 (2020), 36–57. https://doi.org/10.1016/j.jspi.2020.01.007.

[27] J.W. Miller, Lecture Notes on Advanced Stochastic Modeling, Duke University, Durham, NC (2016).

[28] E.G. Simanjuntak, Widiarti, D. Kurniasari, Amanto, Asymptotically Unbiased, Efficient, and Consistent Properties of the Bayes Estimator in the Binomial Distribution with Prior Beta, J. Phys.: Conf. Ser. 1751 (2021), 012019. https://doi.org/10.1088/1742-6596/1751/1/012019.

[29] I.G.N.M. Jaya, F. Kristiani, Y. Andriyana, A. Chadidjah, Sensitivity Analysis on Hyperprior Distribution of the Variance Components of Hierarchical Bayesian Spatiotemporal Disease Mapping, Mathematics 12 (2024), 451. https://doi.org/10.3390/math12030451.

[30] E. Musenge, T.F. Chirwa, K. Kahn, P. Vounatsou, Bayesian Analysis of Zero Inflated Spatiotemporal HIV/TB Child Mortality Data Through the INLA and SPDE Approaches: Applied to Data Observed Between 1992 and 2010 in Rural North East South Africa, Int. J. Appl. Earth Obs. Geoinf. 22 (2013), 86–98. https://doi.org/10.1016/j.jag.2012.04.001.

[31] J.J. Abellan, S. Richardson, N. Best, Use of Space–Time Models to Investigate the Stability of Patterns of Disease, Environ. Health Perspect. 116 (2008), 1111–1119. https://doi.org/10.1289/ehp.10814.

[32] A. Aswi, S.M. Cramb, P. Moraga, K. Mengersen, Bayesian Spatial and Spatio-Temporal Approaches to Modelling Dengue Fever: A Systematic Review, Epidemiol. Infect. 147 (2018), e33. https://doi.org/10.1017/S0950268818002807.